Electronic Supplementary Material (ESI) for Journal of Materials Chemistry C.

Supporting information

Substitution-type luminescent MOFs sensor with built-in capturer for the selective cholesterol detection in blood serums

Ming Gong, Jian Yang, Yongsheng Li, Qixin Zhuang and Jinlou Gu*

Key Laboratory for Ultrafine Materials of Ministry of Education, School of Materials Science and Engineering,

East China University of Science and Technology, Shanghai 200237, China

Fax: +86-21-64250740; Tel: +86-21-64252599

S1. The carboxylation of *β*-CD to *β*-CMCD

The synthetic procedure is demonstrated in Fig. S1. It could be found that the resultant high concentrations of *β*-CMCD powders are easily dissolved in cold water, while the same amounts of *β*-CD powders remain their insolubility. This improved hydrophilicity indicates the existence of the terminal carboxyl groups on *β*-CMCD. The successful modification is further verified through the characteristic FT-IR peaks of carboxymethyl groups in Fig. S2, as well as the more negative zeta potential as shown in Fig. S3.

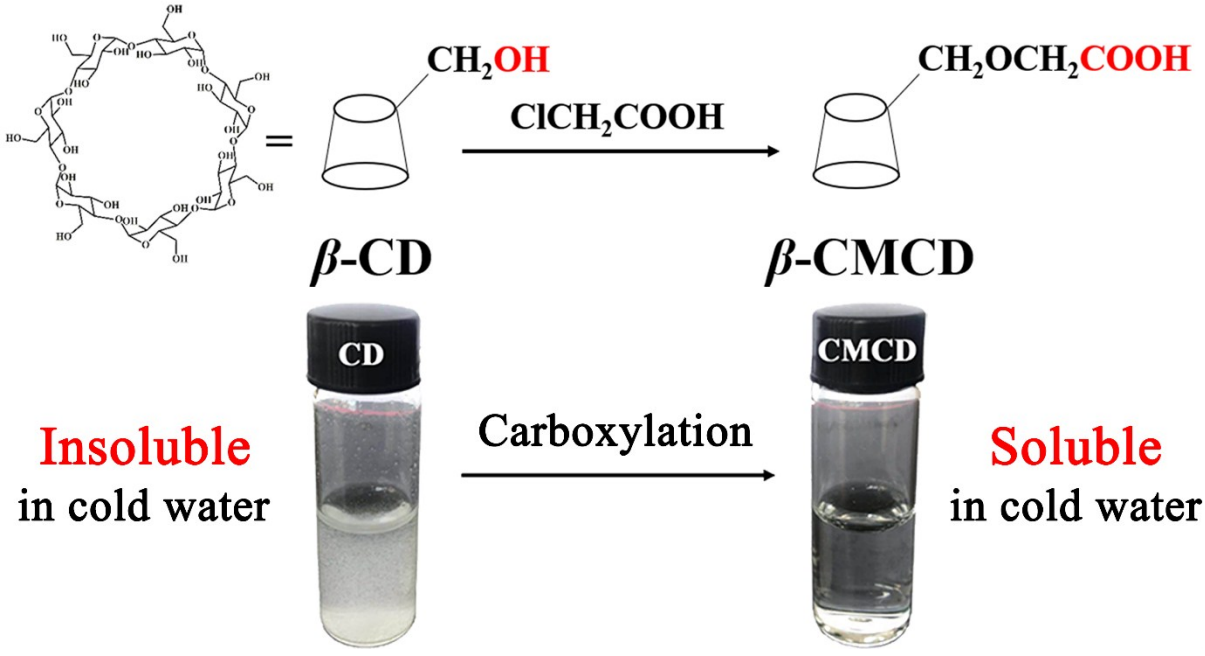

Fig. S1 An illustration for the carboxylation of *β*-CD and the photos of their solubilities in cold aqueous solutions at the concentrations of 20 mg mL^{-1}.

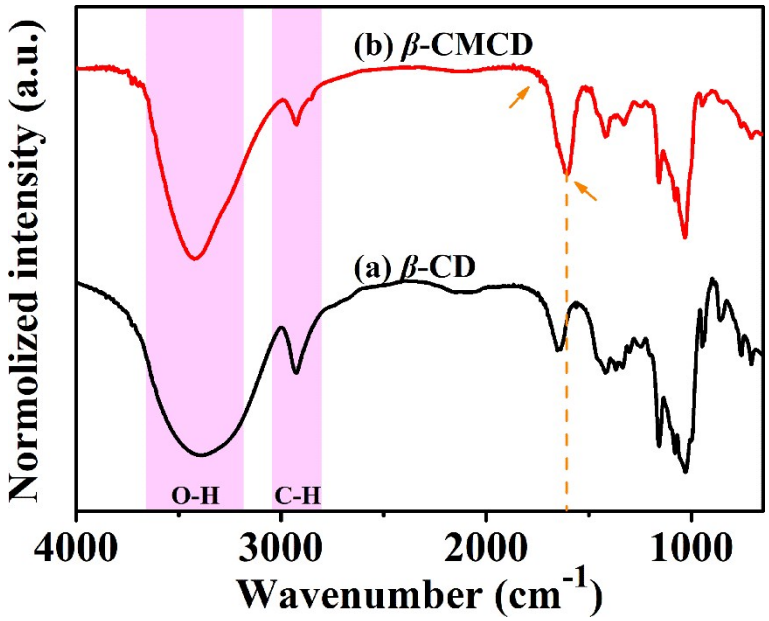

Fig. S2 FT-IR spectra of (a) *β*-CD and (b) *β*-CMCD. The arrows at 1707 and 1598 cm^{-1} in sample (b) represent the C=O stretching vibration of carbonyl groups and C-O-C vibrations, indicating the attachment of carboxymethyl group on *β*-CD.

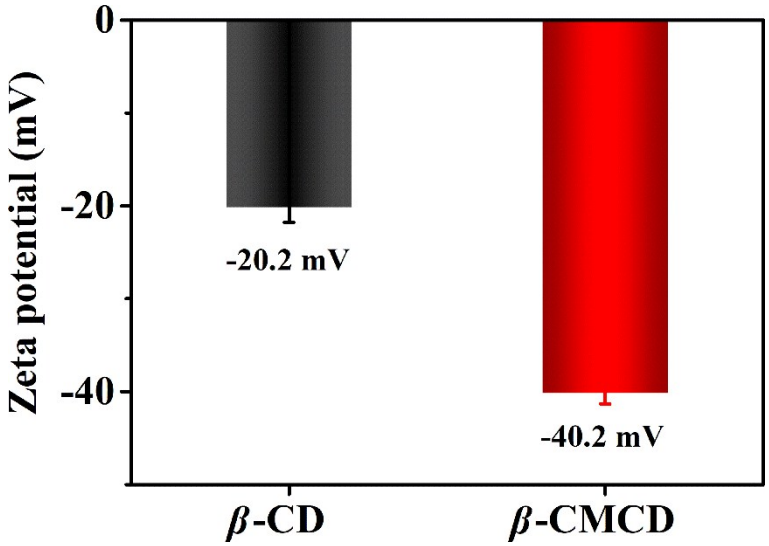

Fig. S3 Zeta potentials of *β*-CD and *β*-CMCD measured in HEPES buffer solution (pH = 7.4).

S2. The quantification of *β*-CMCD in LMOF by TG

The content of *β*-CMCD is further determined by TG in air atmosphere. The heating rate is set as 10 °C/min.

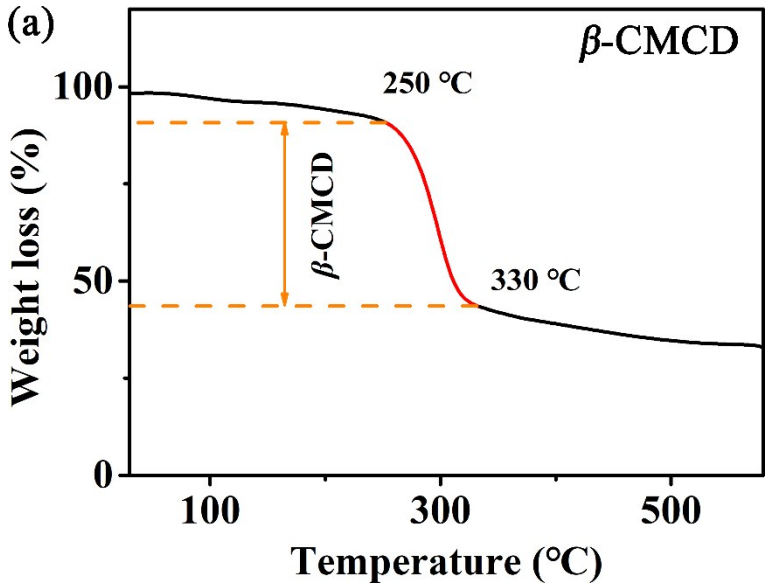

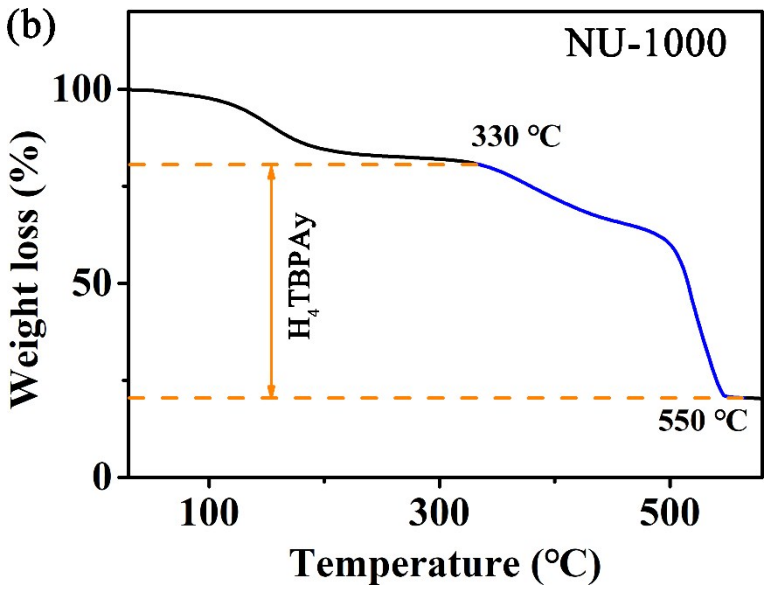
(b)
NU-1000
100
50
0
Weight loss (%)
330 °C
H4TBPAy
550 °C
100
300
500
Temperature (°C)

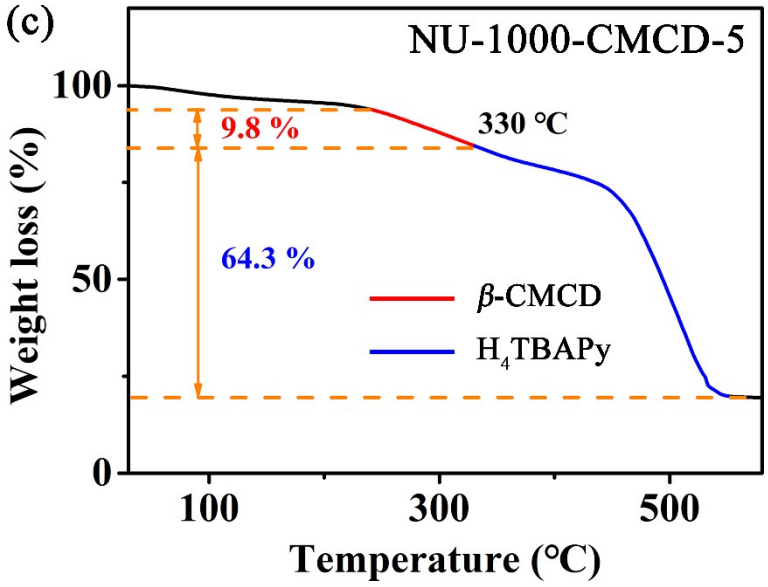
(c)
NU-1000-CMCD-5
100
50
0
Weight loss (%)
9.8 %
330 °C
64.3 %
β-CMCD
H4TBAPy
100
300
500
Temperature (°C)

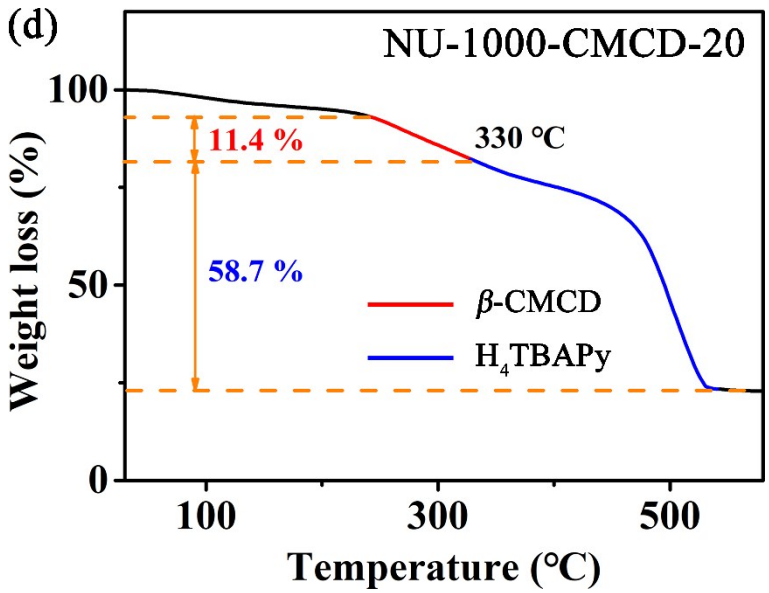

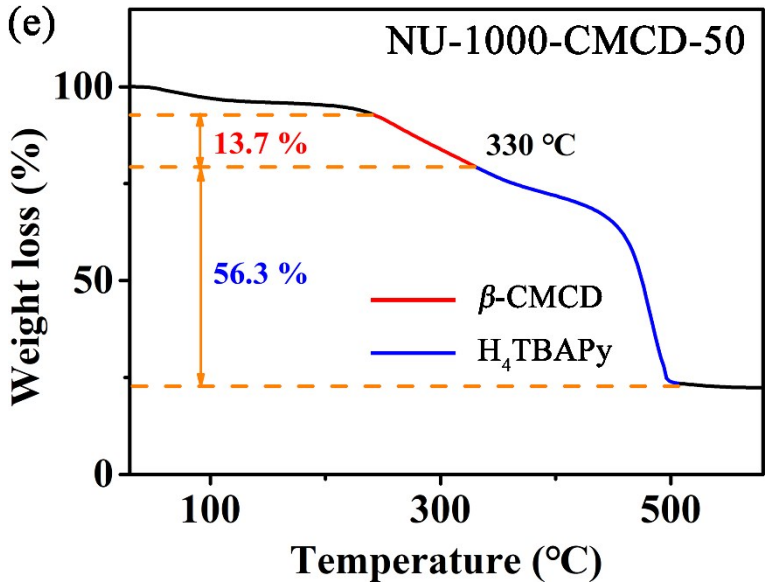

Fig. S4 TG curves for (a) *β*-CMCD, (b) NU-1000, (c) NU-1000-CMCD-5, (d) NU-1000-CMCD-20 and (e) NU-1000-CMCD-50 recorded in a flow of air with the heating rate of 10 °/min.

S3. The grafting stability of *β*-CMCD in LMOF by ^{1}H NMR

The ^{1}H NMR was conducted to confirm the grafting stability of *β*-CMCD in LMOF. 25 mg NU-1000-CMCD was dissolved in D_2O, and the supernatants were collected at 3 d, 5 d, and 7 d after the centrifugation process. The solvent peak for D_2O is identified with (*) at the chemical shift of 4.7 ppm. The curves are also amplified 50 times and inserted upon each spectrum.

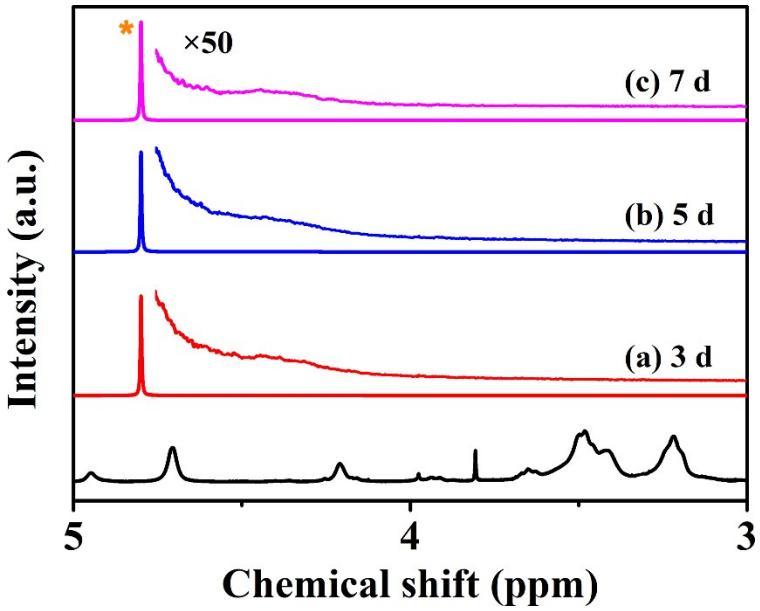

Fig. S5 ^{1}H NMR spectra of the supernatant fraction of NU-1000-CMCD after the placement for (a) 3 d, (b) 5 d and (c) 7 d; the peaks for D_2O is denoted with (*). The black spectrum is the simulated ^{1}H NMR of *β*-CMCD.

S4. The characterization of Rh6G@NU-1000-CMCD

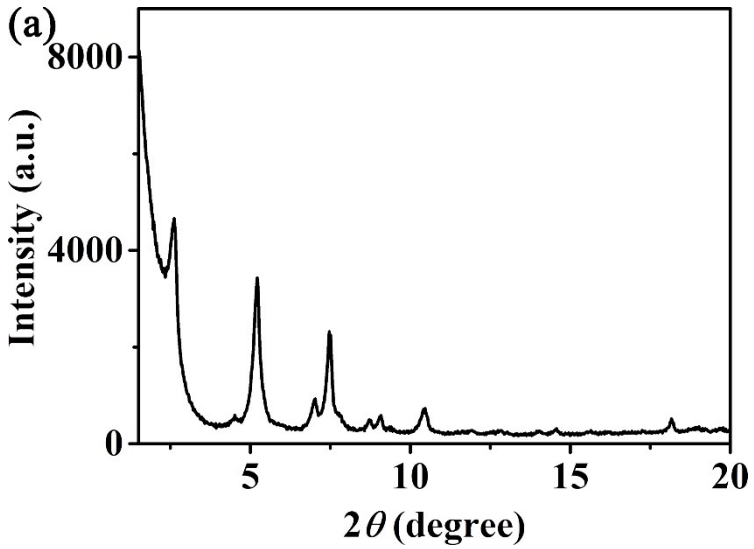

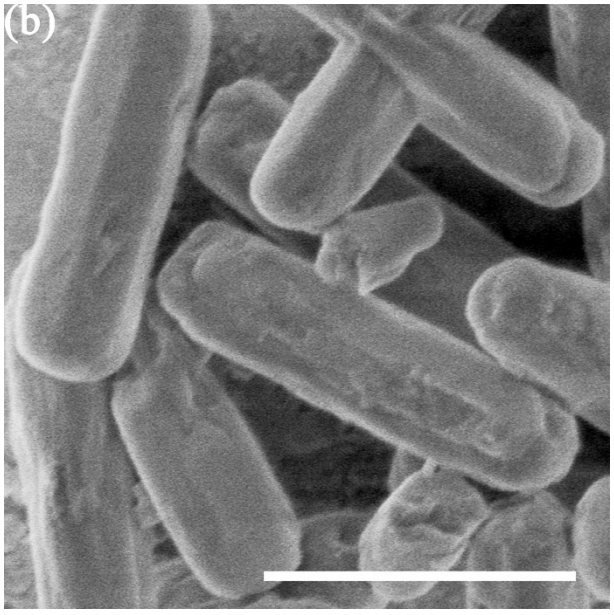

Fig. S6 (a) Powder XRD pattern and (b) SEM image of Rh6G@NU-1000-CMCD. Scale bar: 500 nm.

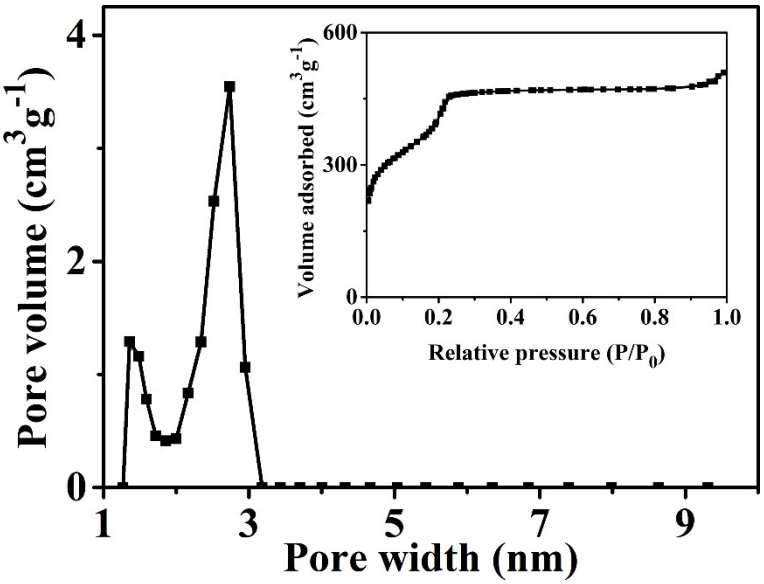

Fig. S7 N_2 sorption isotherm and the corresponding DFT pore size distribution profile (inset) of Rh6G@NU-1000-CMCD measured at 77 K.

Table S1 BET surface areas and pore volumes of the NU-1000-CMCD and Rh6G@NU-1000-CMCD.

LMOFs	Surface area (m^2 g^{-1})	Volume (cm^3 g^{-1})
NU-1000-CMCD	1467	0.88
Rh6G@NU-1000-CMCD	1276	0.78

S5. The optical performances of NU-1000-CMCD and Rh6G@NU-1000-CMCD

To ensure that the introduction of *β*-CMCD would not change the optical performances of NU-1000, the UV-vis and fluorescence spectra of NU-1000-CMCD were recorded, compared with pristine NU-1000 and single *β*-CMCD. Furthermore, after the dye-loading process, the fluorescence spectrum of the Rh6G@NU-1000-CMCD is also measured and its long-time stability is taken into consideration. The sample is dissolved in water for serval days at a concentration of 4 mg mL^{-1}, and three time points (3 d, 5 d and 7 d) are chosen for the fluorescence detection.

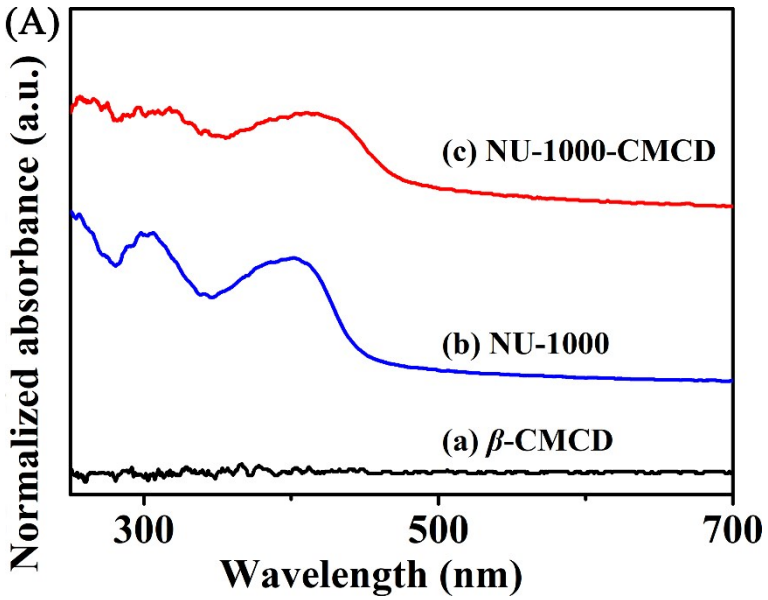

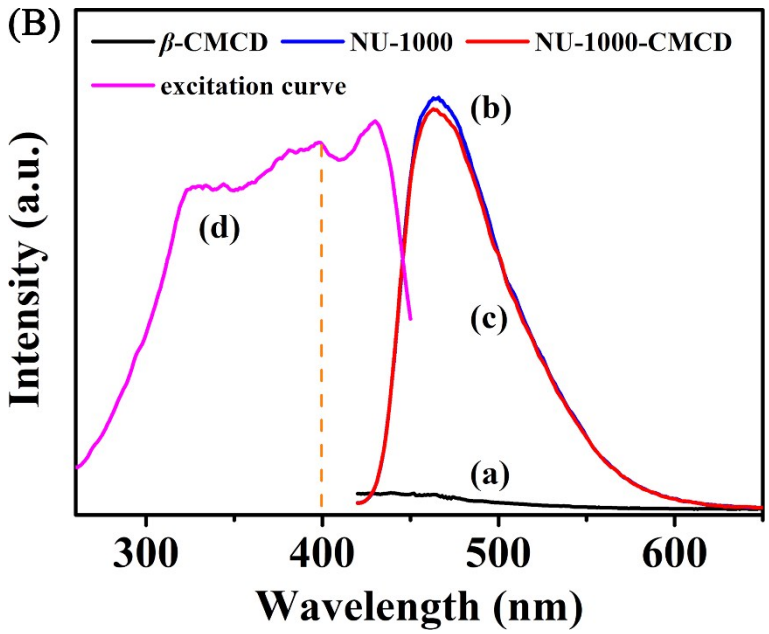

Fig. S8 (A) UV-vis absorbance spectra and (B) fluorescence spectra of (a) *β*-CMCD, (b) NU-1000 and (c) NU-1000-CMCD.

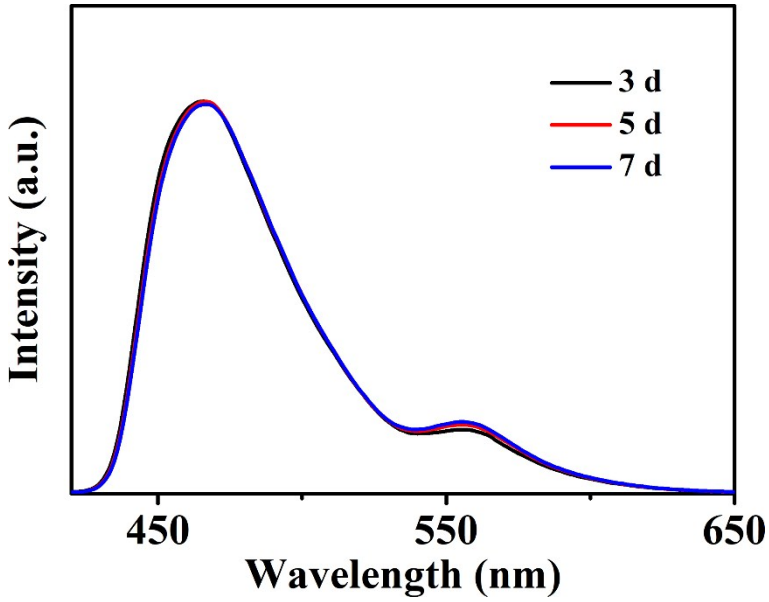

Fig. S9 Fluorescent spectra of the supernatant fraction of NU-1000-CMCD after the placement for (a) 3 d, (b) 5 d and (c) 7 d.

S6. The time-dependence on the cholesterol sensing behavior by Rh6G@NU-

1000-CMCD

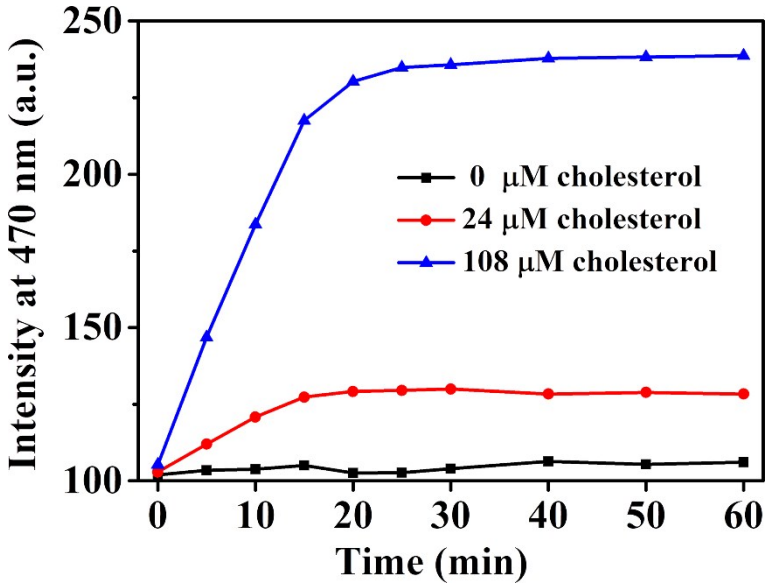

Fig. S10 The effect of incubation time on the fluorescent intensity upon the addition of cholesterol into the Rh6G@NU-1000-CMCD LMOFs sensing system.

The calculation of LOD for cholesterol detection by Rh6G@NU-1000-CMCD:

$$LOD = 3\sigma/slope = 3\times0.17/1.28 = 0.4\ \mu M$$

Sample standard deviation σ for the blank probe, without the addition of cholesterol was calculated to be 1.28.

Table S2 Comparison of the analytical performances of cholesterol sensing systems with different reported methods.

Probes	LOD	Linear range	Enzyme	Response time	References
β-CD-CQD, p-nitrophenol	0.7 μM	0-110 μM	Free	42 min	1
RB-CD-Cit-UCNPs	3 μM	10-110 μM	Free	40 min	2
Au@CDs	2.5 μM	1-6.25 mM	Free	30 min	3
BSA-AuNCs	1.4 μM	1-100 μM	ChOx	1 h	4
PCN-333/RhB-ChOx	0.6 μM	0-40 μM	ChOx	40 min	5
ChOx-Fe3O4@MIL-100(Fe)	0.8 μM	0-50 μM	ChOx	1 h	6
ChOx-MOF-5/AgNC/MoS2	0.03 μM	0.06-15 μM	ChOx	10 min	7
Rh6G@NU-1000-CMCD	0.4 μM	0-108 μM	Free	30 min	This work

S7. The quantitative analysis of Rh6G in the Rh6G@NU-1000-CMCD probe.

To analyze the Rh6G amounts in LMOF, the absorbances of standard solutions of

Rh6G was plotted by linear fitting of the absorbance at 525 nm. The LMOF suspension was set up at a concentration of 5.5 mg per 5 mL NaOH solution.

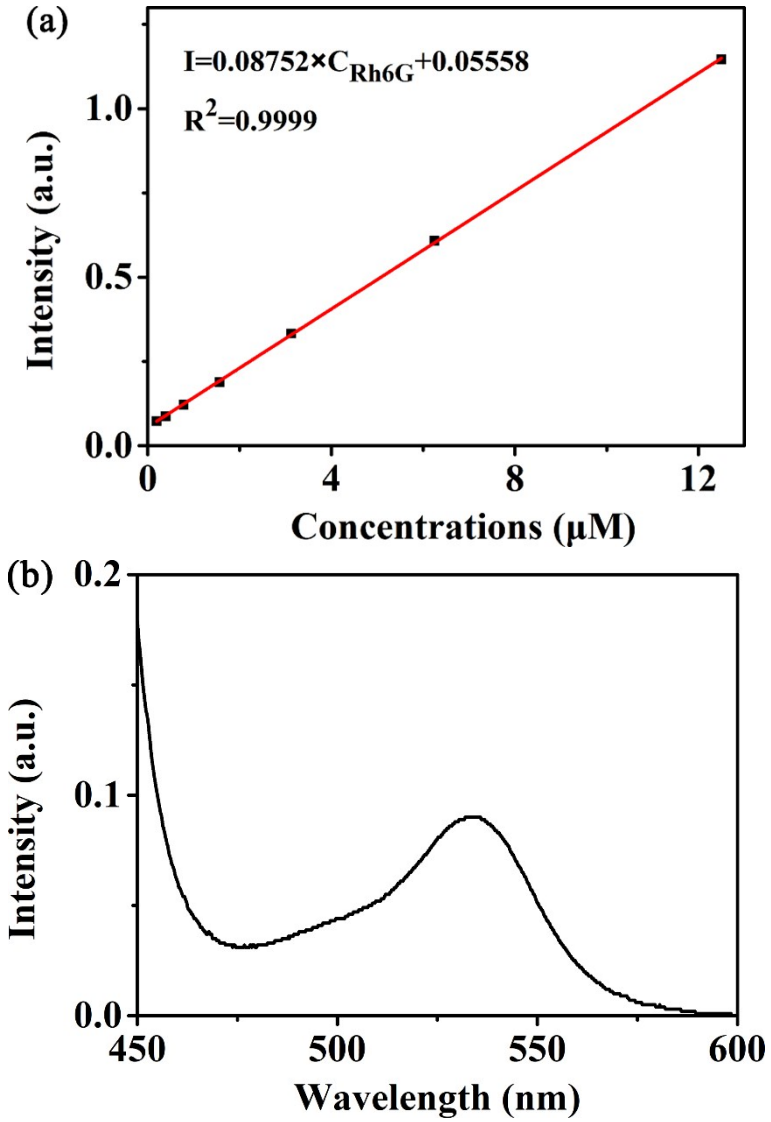

Fig. S11 (a) Linear fitting of Rh6G absorbance at 530 nm. (b) UV-vis spectrum of degraded Rh6G@NU-1000-CMCD.

S8. The fluorescence spectra supporting for the sensing mechanism

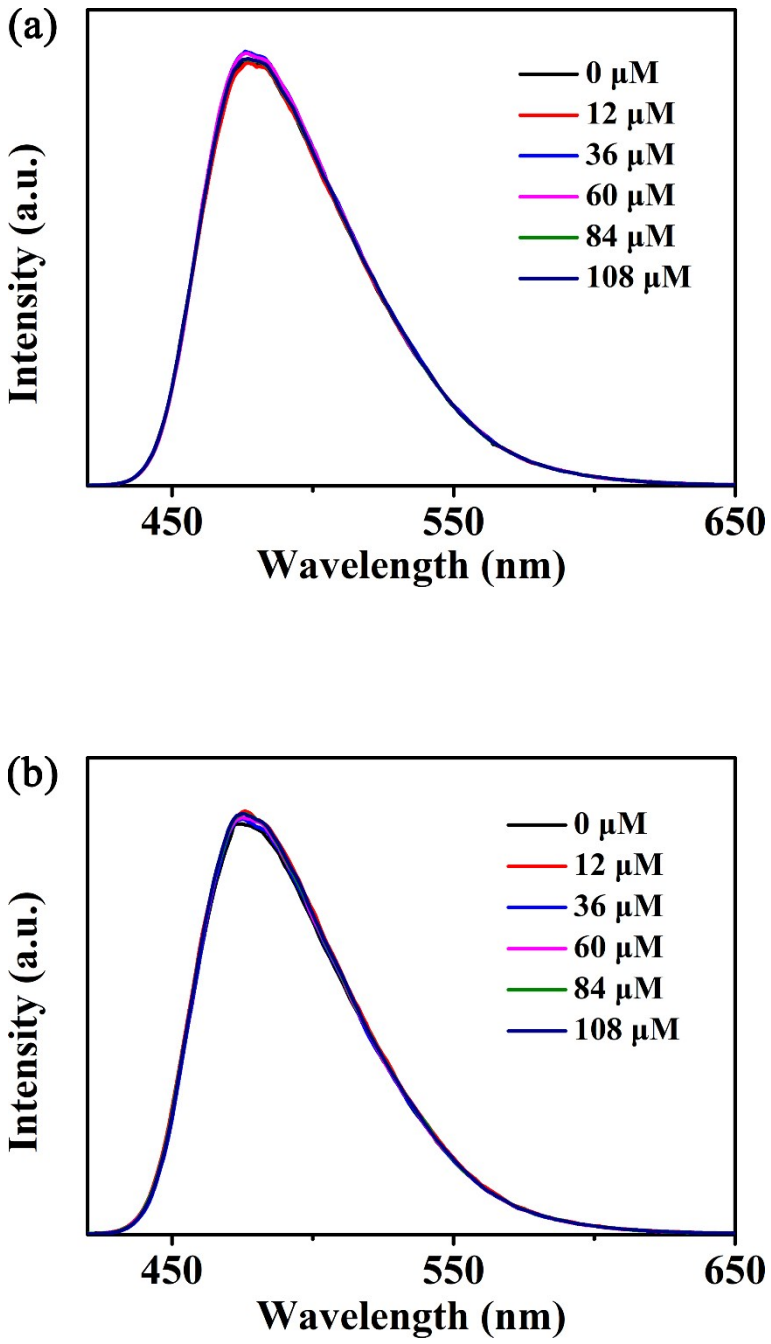

Fig. S12 Fluorescent spectra of (a) NU-1000 and (b) NU-1000-CMCD after the addition of different concentrations of cholesterol under excitation at 400 nm.

S9. The reversible sensing for cholesterol

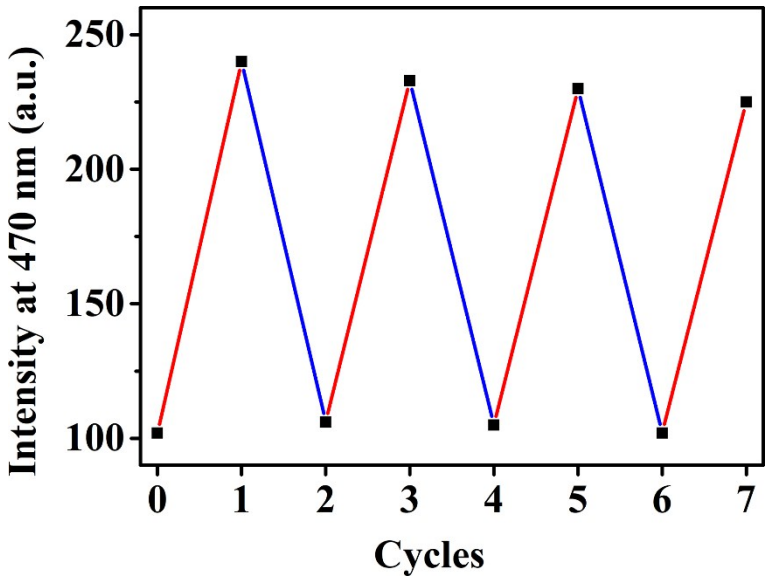

Fig. S13 Fluorescent intensity at 470 nm to demonstrate the reversibility of the Rh6G@NU-1000-CMCD sensor for cholesterol detection. The red curves show cholesterol-sensing process and the blue curves show the hexane-washing and Rh6G-reloading processes.

References

1 Q. Sun, S. Fang, Y. Fang, Z. Qian and H. Feng, *Talanta*, 2017, **167**, 513.

2 Y. Ding, H. Zhu, X. Zhang, J. Gao, E. -S. Abdel-Halim, L. Jiang and J. -J. Zhu, *Nanoscale*, 2014, **6**, 14792.

3 N. Zhang, Y. Liu, L. Tong, K. Xu, L. Zhuo and B. Tang, *Analyst*, 2008, **133**, 1176.

4 H. -C. Chang and J. A. Ho, *Anal. Chem.*, 2015, **87**, 10362.

5 M. Zhao, Y. Li, X. Ma, M. Xia and Y. Zhang, *Talanta*, 2019, **200**, 293.

6 Y. Wu, Y. Ma, G. Xu, F. Wei, Y. Ma, Q. Song, X. Wang, T. Tang, Y. Song, M. Shi, X. Xu and Q. Hu, *Sens. Actuators, B*, 2017, **249**, 195.

7 J. Hassanzadeh, A. Khataee and H. Eskandari, *Sens. Actuators, B*, 2018, **259**, 402.